nature communications

Article

https://doi.org/10.1038/s41467-024-52328-z

Passive isothermal film with self-switchable radiative cooling-driven water sorption layer for arid climate applications

Received: 26 March 2024

Accepted: 27 August 2024

Published online: 12 September 2024

Check for updates

Seonggon Kim[1], Sunghun Lee[1,2], Jehyung Lee[1,2], Hyung Won Choi[1,2], Wonjoon Choi[2] & Yong Tae Kang[1,2]

Reducing substantial energy demand of active heating, ventilation, and air conditioning in arid climates is of paramount importance. Here, we develop a millimeter-scale passive isothermal film that maintains temperature near 25 °C without relying on energy consumption solely through natural phenomena. A radiative cooling unit comprising polydimethylsiloxane (PDMS) with diffraction grating and fused SiO_2/Ti/Ag film facilitates radiative cooling during daylight hours. Net thermal energy is stored through water desorption of porous materials (latent cooling) and dissolution of ammonium nitrate in water (endothermic reaction). At nighttime, thermal emission is suppressed by the destructive interference of PDMS diffraction, and thermochemical reverse reaction occurs to sustain temperature in response to heat loss from the ambient environment. It reduces cooling and heating loads by approximately −1.1 and 0.3 kW m^{-2}, respectively, throughout a full day. Our results indicate the potential of designing a passive system suitable for human habitation without an active system.

City construction projects are currently underway in arid regions, where energy consumption for heating, ventilation, and air conditioning (HVAC) presents a significant challenge[1]. These areas experience daytime temperatures as high as 60 °C due to exposure to intense sunlight, and rapid temperature drops to below freezing occur after sunset, given the low moisture content and low specific heat of the air. To maintain indoor conditions at 25 °C with 50% relative humidity suitable for human habitation, a cooling load of −42.8 kJ kg_{air}^{-1} is necessary during the daylight hours (when outside air is at 60 °C with a relative humidity of 10%), and a heating load of 59.8 kJ kg_{air}^{-1} is required during the night (when outside air temperature is −10 °C with a relative humidity of 20%). Relying on an active HVAC system to provide heating and cooling would result in an impractical energy demand. Therefore, the motivation is to develop a passive film that can maintain a human-friendly environment at 25 °C in arid climates using only natural processes without additional energy consumption.

In response to the challenge of reducing excessive cooling loads associated with active systems during the daylight hours, passive cooling methods that offer a sustained cooling effect without energy consumption have been discussed (efficiently utilizing cooling energy is inherently more challenging than heating, as observed from the second law of thermodynamics). Raman et al.[2] reported lowering temperatures by 4.9 °C compared to ambient air using a photonic radiative cooler composed of SiO_2/HfO_2/Ag/Ti_2. However, the high manufacturing cost of this film remains a limiting factor, attributed to the process of depositing sublayers through electron beam evaporation. Recent efforts have focused on cost-effective solutions including hierarchically structured polymethyl methacrylate[3], polydimethylsiloxane-coated metal structure[4], delignification of wood[5], and 3D porous cellulose acetate matrix with internally deposited SiO_2[6]. Additionally, researchers have explored radiative cooling integrated with water harvesting[7] or photovoltaic cells[8]. Passive cooling methods that rely on thermochemical reactions

[1]Research Center for Plus Energy Building Innovative Technology, 145 Anam-ro, Seongbuk-gu, Seoul 02841, Republic of Korea. [2]School of Mechanical Engineering, Korea University, 145 Anam-ro, Seongbuk-gu, Seoul 02841, Republic of Korea. e-mail: ytkang@korea.ac.kr

are studied, rather than radiative phenomena. For instance, alternative latent cooling is demonstrated based on the ambient moisture sorption-desorption behavior of metal-organic frameworks[9]. Other approaches involve the use of hard carbon nanotube sponges[10] and transparent insulation bilyaer[11]. In the previous research of our groups, the cooling power and energy density is significantly improved through a water desorption-driven endothermic reaction of ammonium nitrate[12]. Furthermore, discussions have included various approaches, such as phase change materials[9,10,12], heat pipe[13,14], and thermal superinsulation materials[15–17].

Passive heating methods include direct gain of solar energy such as natural heating[18] and Trombe wall[19], and natural ventilation[20]. However, these methods require a thermal reservoir available outside, which limits their application in arid regions during the nighttime when outdoor temperatures significantly drop below indoor conditions. Although efforts to address the time gap between the supply and demand of thermal energy in building applications have led to the development of energy storage systems[5,18,19,21,22], they involve complex components and low cost-effectiveness. In summary, the passive cooling approaches could reduce daytime temperatures in arid climates[23–25]. However, no passive film has been proposed to mitigate nighttime heating loads without relying on a thermal reservoir. Moreover, when a passive radiative cooling film is solely employed, nighttime heat loss can be substantial, given that the thermal emission power of such films can reach 366 W m^{-2} with an average emissivity/absorptivity close to 1 at room temperature.

Here we develop a millimeter-scale passive isothermal film that incorporates a radiative cooling unit and a water desorption-driven endothermic reaction (WD-ER) unit, permanently maintaining temperature near 25 °C in arid climates. This film utilizes natural processes without any energy consumption and can offset approximately 1100 W m^{-2} of heating power generated during the daylight hours and the −300 W m^{-2} of cooling power during the night, based on its self-switchable characteristics.

Results

Working principle of passive isothermal film

Figure 1a displays a passive isothermal film composed of a low-density polyethylene, a radiative cooling unit containing polydimethylsiloxane (PDMS) with a diffraction grating and fused SiO_2/Ti/Ag sublayers, and a WD-ER unit including chromium(III) terephthalate metal-organic frameworks (MIL-101(Cr)), water, and ammonium nitrate. When external heat is supplied during the daylight hours, the film absorbs some energy (charging), and during the nighttime when outside temperatures drop rapidly, it releases heat (discharging) to maintain a steady 25 °C temperature throughout the day, as illustrated in Fig. 1b.

Figure 1c illustrates the operational mechanism of the passive isothermal film during the daylight hours. The low-density polyethylene layer minimizes forced/natural convection heat transfer through intermittent air. The PDMS diffraction grating predominantly allows solar irradiation to pass through, while the SiO_2/Ti/Ag layers reflect it to prevent overheating. The PDMS diffraction grating is designed to achieve an emissivity close to 1.0 within the temperature range of 30–60 °C (typical of daytime temperatures in arid climates), enabling thermal emission cooling. The WD-ER unit

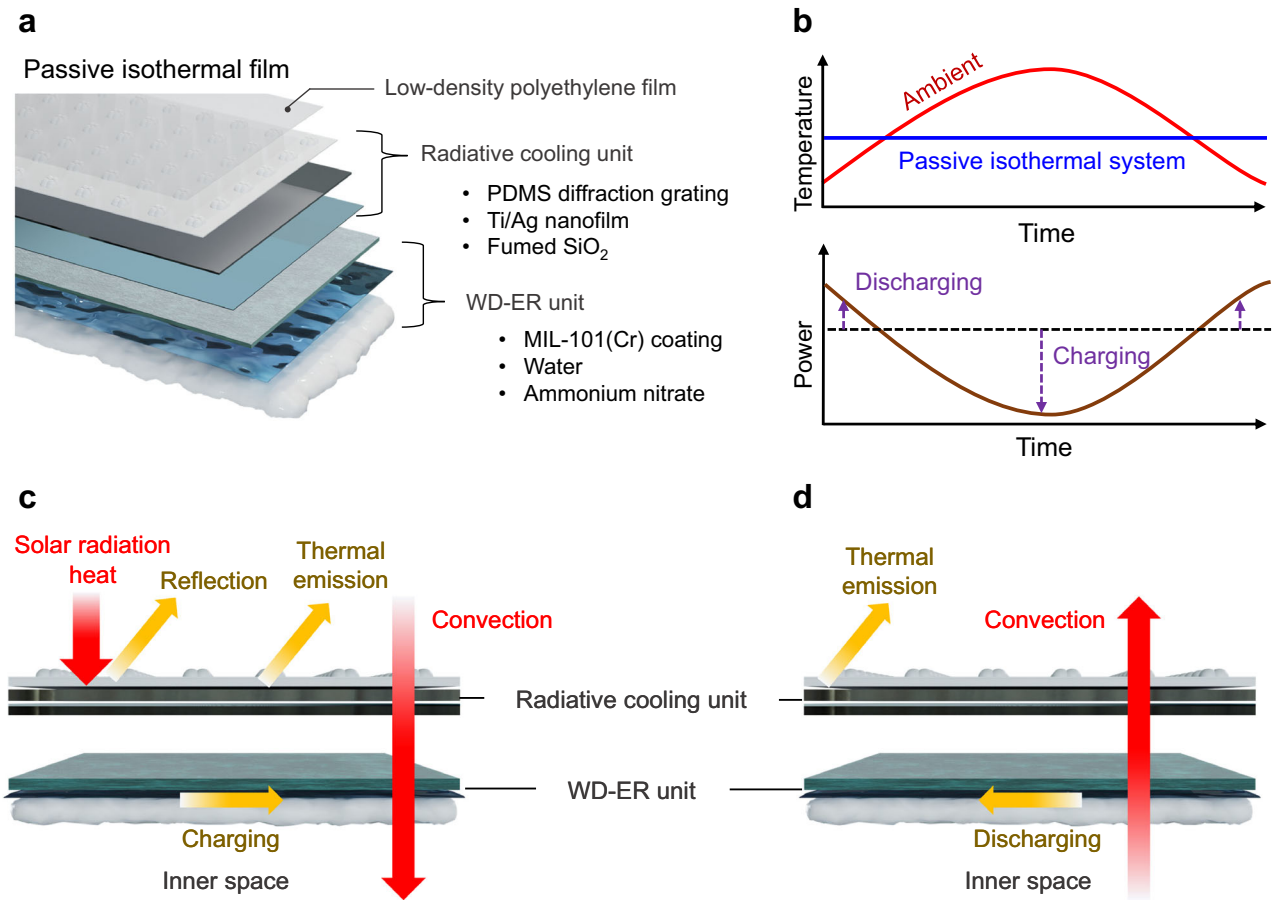

Fig. 1 | Schematic description of the passive isothermal film. a Configuration of the system consisting of radiative cooling and water desorption-driven endothermic reaction (WD-ER) layers for arid climates. **b** Theoretical cooling and heating power to maintain an isotherm of 25 °C throughout a full day. **c** Cooling mechanism during daylight hours. **d** Heating mechanism during nighttime. PDMS and MIL-101(Cr) represent the polydimethylsiloxane and chromium(III) terephthalate metal-organic frameworks, respectively.

absorbs the net thermal energy input through a chain reaction, involving water desorption from the MIL-101(Cr) coating layer for latent cooling and an endothermic reaction by dissolution of ammonium nitrate in water. This process sustains indoor temperatures by utilizing the principles that the water sorption capacity of porous materials decreases as temperature increases and the solubility of solutes rises with temperature. During the nighttime, when the PDMS diffraction grating is exposed to lower outdoor temperatures than indoors, its emissivity significantly decreases, minimizing thermal emission heat loss as illustrated in Fig. 1d. Additionally, the reverse reaction in the WD-ER unit releases heat, which aids the temperature maintenance.

While the conventional passive radiative cooling systems focused on minimizing solar irradiation (reducing absorptivity in the ultraviolet-visible (UV-Vis) range) and enhancing thermal emission power (achieving emissivity close to 1 in the infrared spectrum), in this study, some energy input from nature is utilized to operate the WD-ER unit to store energy during daylight hours. It enables the passive isothermal system to discharge the stored energy during the nighttime, which minimizes heating and cooling energy loads in arid climates, utilizing the diurnal energy balance.

For a deeper reflection on the physical working principle in quasi-steady state, the energy conservation equation for the passive isothermal film during daylight hours is described by Eq. (1). The left-hand term represents the sensible heat change of the film, where m is mass, c_p is specific heat capacity, T is temperature, and t is time, respectively. The solar irradiation power ($\dot{Q}_{sun}$) is defined by Eq. (2), and the emissivity (ε) and absorptivity are identical in thermal equilibrium based on Kirchhoff's law of thermal radiation, where A represents surface area, Θ denotes the angle of incidence, λ stands for the wavelength of electromagnetic waves, and I_{AM} represents solar illumination:

$$\sum m \cdot c_p \cdot \Delta T = \int (\dot{Q}_{sun} + \dot{Q}_{amb} - \dot{Q}_{rad} + \dot{Q}_{conv} - \dot{Q}_{in})\mathrm{d}t - Q_{cg} \quad (1)$$

$$\dot{Q}_{sun} = A \int \varepsilon(\lambda, \theta_{sun}) \cdot I_{AM}(\lambda) \cdot \mathrm{d}\lambda \quad (2)$$

The irradiation power from the atmosphere, $\dot{Q}_{amb}$ is given by Eq. (3), where $\int \mathrm{d}\Omega$ represents the angular integral over the surface, and the subscript amb denotes the ambient air. The thermal emission of blackbody (I_B) is governed by the Planck's law described by Eq. (4). h represents Planck's constant, c is the speed of light, and k is Boltzmann constant, respectively:

$$\dot{Q}_{amb} = A \int \cos\theta \cdot \mathrm{d}\Omega \int I_B(T_{amb}, \lambda) \cdot \varepsilon(\lambda, \theta) \cdot \varepsilon_{amb}(\lambda, \theta) \cdot \mathrm{d}\lambda \quad (3)$$

$$I_B = \frac{2hc^2}{\lambda^5} \cdot \frac{1}{\exp(hc/\lambda kT - 1)} \quad (4)$$

The thermal radiation from the surface, $\dot{Q}_{rad}$ is described by Eq. (5). $\dot{Q}_{conv}$ accounts for the heat transferred through the medium as in Eq. (6), considering forced/natural convective heat transfer coefficient by intermittent air (h_{air}) and the thermal resistances related to conduction within the passive isothermal film. The natural convective heat transfer between the passive isothermal film and the air inside the inner space ($\dot{Q}_{in}$) is given by Eq. (7):

$$\dot{Q}_{rad} = A \iint \cos\theta \cdot I_B(T, \lambda) \cdot \varepsilon(\lambda, \theta)\mathrm{d}\Omega\mathrm{d}\lambda \quad (5)$$

$$\dot{Q}_{conv} = h_{air} \cdot A \cdot (T_{amb} - T) \quad (6)$$

$$\dot{Q}_{in} = h_{in} \cdot A \cdot (T - T_{in}) \quad (7)$$

The heat absorbed by the radiative cooling unit is equivalent to the heat sink term (Q_{cg}) in the WD-ER unit during the charging process of daylight hours. It includes the latent heat absorption from water desorption in MIL-101(Cr), Q_d, as described in Eq. (8) and the endothermic heat absorption from ammonium nitrate dissolution, Q_e, as in Eq. (9), where m_a represents the mass of MIL-101(Cr), h_d is the average specific enthalpy of water desorption, and x_w denotes the adsorption capacity of the adsorbent at a specific temperature. m_w represents the mass of water, h_e is the average specific enthalpy of ammonium nitrate dissolution, and x_n stands for the solubility of water:

$$Q_d = m_a \cdot h_d \cdot (x_{w,i} - x_{w,i+1}) \quad (8)$$

$$Q_e = m_w \cdot h_e \cdot (x_{n,i+1} - x_{n,i}) \quad (9)$$

The energy conservation equation during the nighttime is represented by Eq. (10), where Q_{dcg} denotes the heat source (discharging) term for the WD-ER unit:

$$\sum m \cdot c_p \cdot \Delta T = \int (\dot{Q}_{amb} - \dot{Q}_{rad} - \dot{Q}_{conv} + \dot{Q}_{in})\mathrm{d}t + Q_{dcg} \quad (10)$$

Radiative cooling unit

Field emission scanning electron microscopy (FE-SEM) images of the PDMS diffraction grating are presented in Fig. 2a. The grating incorporates protrusion shapes with 3.25 μm in width and height, spaced at 8 μm intervals. It facilitates the generation of thermal emission within a specific temperature range of 30–60 °C, corresponding to the daylight hours in arid climates. Additionally, it suppresses thermal emission in the temperature range of 0–10 °C during the nighttime hours. Constructive interference of electromagnetic waves (resonance) is induced at wavelength of 8–9 μm, while destructive interference occurs at the wavelength of 10–11 μm. Figure 2b presents the FE-SEM images of an Ag film deposited on fused SiO_2 wafer with thickness of 525 μm. Ti layer with thickness of 10 nm was deposited between the silica nonpolar surfaces and the Ag film to enhance interfacial adhesion. Energy dispersive spectroscopy (EDS) confirms the surface composition as fused SiO_2/Ti/Ag. The thickness of Ag film is 250 nm, which can be treated as bulk Ag as the penetration depth of infrared (IR) electromagnetic waves is on the order of tens of nanometers.

Figure 2c presents the optical characteristics in the ultraviolet-visible-near infrared (UV-Vis-NIR) region of the radiative cooling unit, consisting of fused SiO_2/Ti/Ag and PDMS diffraction grating. The maximum peak of solar irradiance was normalized to the order of absorptivity. The detailed data in terms of PDMS thickness is presented in Figs. S1–S6. The average absorptivity of PDMS to solar irradiance is 0.0584, and the reflectance of the fused SiO_2/Ti/Ag film exceeds 0.9. The net solar thermal energy absorbed by the radiative cooling unit is equivalent to 78.8 W m^{-2}, assuming solar standard spectrum air mass of 1.5. While previous studies have reported radiative coolers with superior solar energy reflection performance[25–28], this study has focused on the passive isothermal system, which requires absorbing some solar thermal energy to maintain almost constant temperature through the nighttime discharging. Figure 2d illustrates the absorptivity/emissivity of the radiative cooling unit in the IR region. Constructive interference results in the emissivity close to 1 at 9.2 μm, corresponding to the peak of black body emission at 40 °C, whereas emissivity converges to 0 due to destructive interference at 10.2 μm of peak emission at 10 °C. The thermal emissions of black body at 10 °C

https://doi.org/10.1038/s41467-024-52328-z

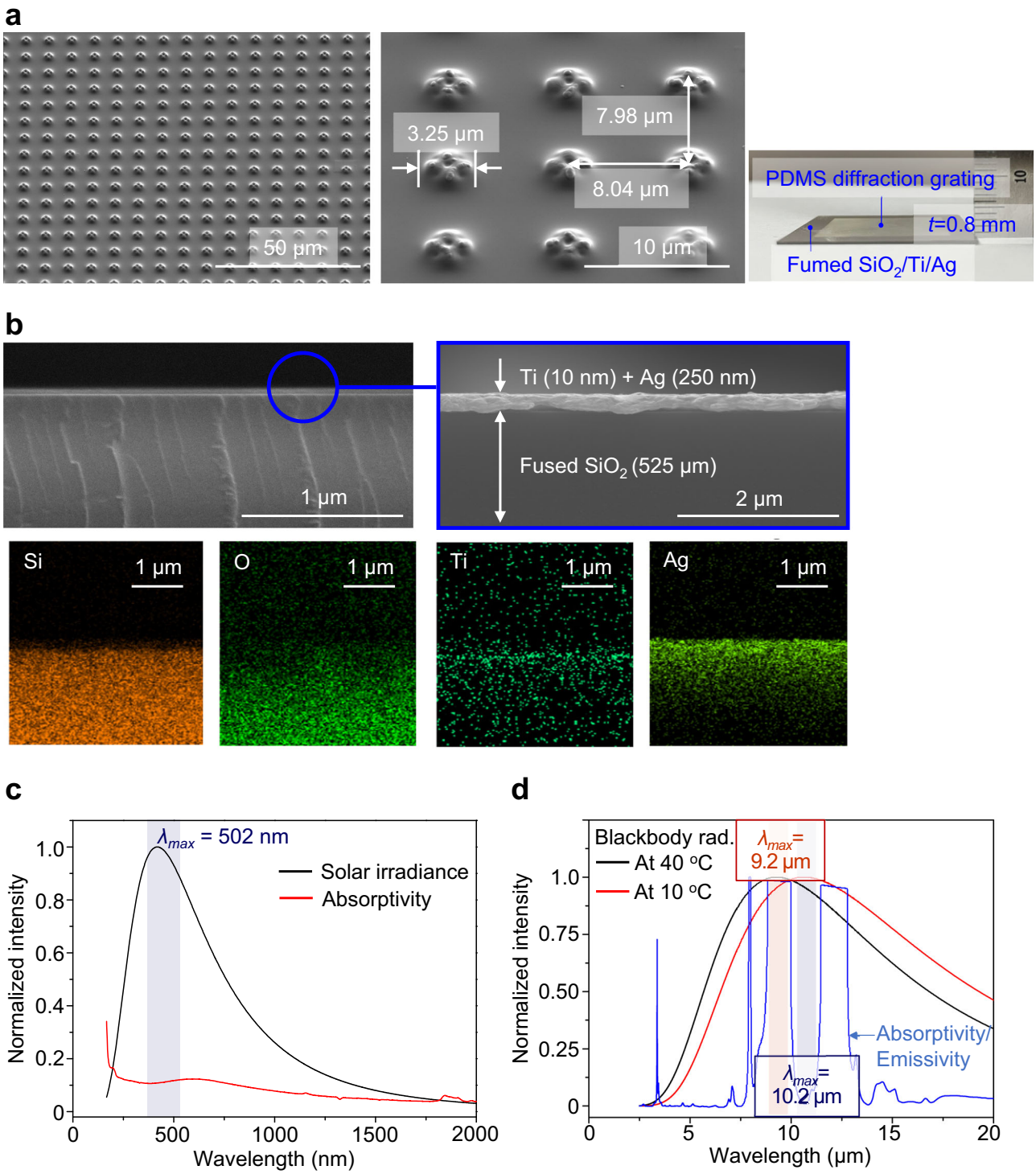

Fig. 2 | Characteristics of the radiative cooling unit. a Field emission scanning electron microscopy (FE-SEM) images of the polydimethylsiloxane (PDMS) diffraction grating. **b** FE-SEM images and energy dispersive spectroscopy (EDS) of the fused SiO_2/Ti/Ag sublayers. **c** Normalized solar irradiance and absorptivity/emissivity of the radiative cooling unit in the ultraviolet-visible-near infrared (UV-Vis-NIR) region. **d** Normalized thermal emission from a black body and absorptivity/emissivity of the radiative cooling unit in the infrared region. *t* is the thickness of the radiative cooling unit. λ_{max} represents the maximum wavelength of electromagnetic wave at a specific temperature. Source data are provided as a Source Data file.

and 40 °C are 366 and 547 W m^{-2}, respectively. However, the radiative cooling unit effectively reduces these to 186 and 131 W m^{-2}, respectively. This enables appropriate thermal energy charging during the daylight hours and minimizes heat loss due to thermal emission at night. The surface states of the radiative cooling unit are analyzed using X-ray photoelectron spectroscopy (XPS) in Fig. S7a. As the radiative cooling unit does not suffer oxidative degradation, only silicon, carbon, and oxygen are detected, which are components of PDMS. On the other hand, the structural phase purity is observed through X-ray diffraction (XRD) in Fig. S7b.

Figure 3a illustrates the experimental setup used to evaluate the practical performance of the radiative cooling unit. SiO_2/Ti/Ag

https://doi.org/10.1038/s41467-024-52328-z

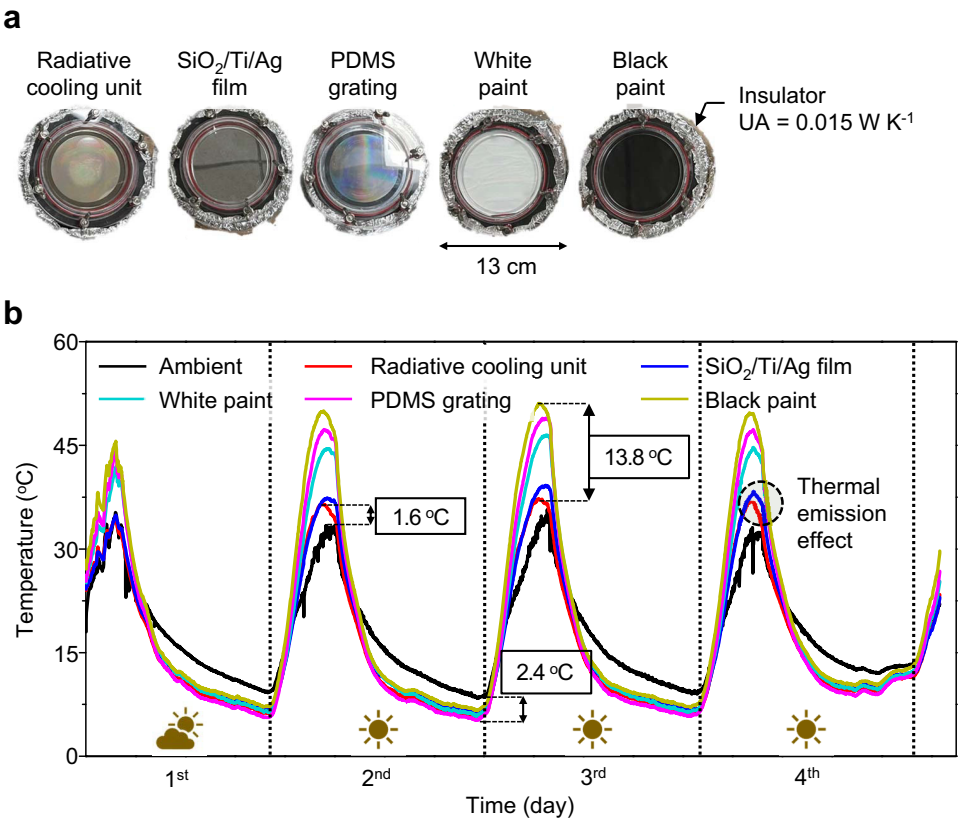

Fig. 3 | Practical performances of the radiative cooling unit. a Images of the experimental apparatus. **b** Temperature variation in terms of materials throughout a full day. UA and PDMS represent the overall heat transfer coefficient of the insulating materials and the polydimethylsiloxane, respectively. Source data are provided as a Source Data file.

film, PDMS diffraction grating, white paint, and black paint were utilized as the comparison groups (see Fig. S8). The temperature of outdoor air fluctuates significantly, ranging from 8.4 °C to 35.7 °C. Note that the outdoor temperature was measured at the base camp with a roof based on the objective of constructing an indoor passive isothermal system. Black paint exhibits the highest absorption of solar energy during the daylight hours, resulting in a maximum temperature of 51 °C. The PDMS diffraction grating presents high thermal emission, however, the temperature rises significantly due to the transmission of most of the solar energy into the interior space. The temperature of the radiative cooling unit is 1.6 °C higher than the ambient temperature, and it reduces temperature by 1–2 °C compared to the SiO_2/Ti/Ag film due to thermal emission. Despite efforts to reduce emissivity in the wavelength range of 10–11 µm, the temperature of the passive cooling unit drops to 5.6 °C during the nighttime, resulting in a maximum temperature difference of 31.7 °C. Cooling is more challenging than heating from a thermodynamic perspective. However, heating to compensate for heat loss may consume more energy in regions where the temperature fluctuates significantly.

Water desorption-driven endothermic reaction unit

Figure 4a presents the FE-SEM image of MIL-101(Cr). The particles exhibit an angular structure due to the micropores and they are distributed in the range from 300 to 500 nm. The EDS detects the presence of both chromium and oxygen, which indicates a combination of organic ligands and metal ions. The micropores of MIL-101(Cr) can be observed in the transmission electron microscope images as presented in Fig. S9a. The XPS and XRD data of MIL-101(Cr) are Fig. S9b, c, respectively. In Fig. 4b, the N_2 adsorption curve of MIL-101(Cr) presents a rapid increase in the relative pressure range of 0–0.25, which confirms the presence of micropores. The surface area calculated by Brunauer–Emmett–Teller theory is 2925 $m^2 g^{-1}$, with a pore size of 1.97 nm based on the Barrett–Joyner–Halenda method. Figure 4c illustrates the isothermal water sorption of MIL-101(Cr), as relative humidity is set to 90%. As the passive isothermal film operates in a moisture-containing environment, the capture capacity depending on the temperature variation is examined at a point where the relative pressure is close to 1. MIL-101(Cr) exhibits water sorption capacity of 1.12 g g^{-1} at 20 °C, and as the temperature rises to 40 °C, approximately 0.434 g g^{-1} of water is desorbed (It is calculated from the chemical equilibrium state. However, WD-ER unit operates in a quasi-steady state with full-day cycle.). Linear regression of the isothermal water sorption capacity enables the prediction of working capacity with respect to temperature changes. The average water desorption enthalpy reaches 53 kJ mol^{-1}. The dynamic vapor sorption curve of MIL-101(Cr) is analyzed at 23 °C as in Fig. 4d, when the relative humidity changes from 0 to 90%. After 10 cycles, the degradation of water sorption capacity is only 0.56% within the reasonable error range (dynamic vapor sorption cycles of other porous materials are presented in Fig. S10). Figure 4e displays the solubility of ammonium nitrate in water as a function of temperature. The dissolution enthalpy for ammonium nitrate is 28.1 kJ mol^{-1}, and its solubility can be fitted with an exponential function. Note that the water capture capacity of porous materials decreases as the temperature rises, resulting in a latent cooling effect during desorption. Simultaneously, the solubility of the solute increases with temperature increase, leading to an endothermic reaction.

The heat dissipation performance of the WD-ER unit was evaluated utilizing the apparatus presented in Fig. S11. Figure 5a illustrates

https://doi.org/10.1038/s41467-024-52328-z

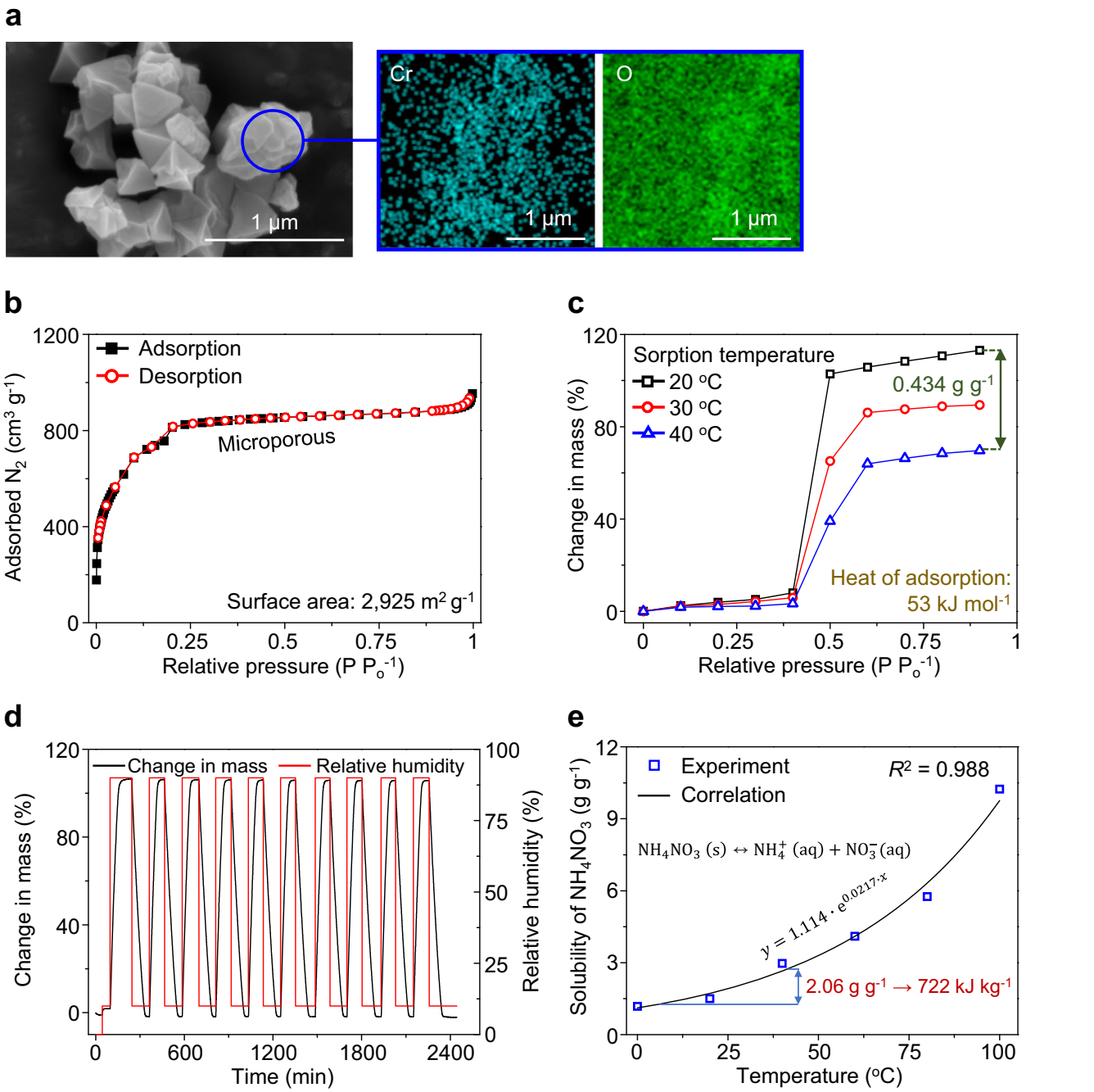

Fig. 4 | Characteristics of the water desorption-driven endothermic reaction (WD-ER) unit. a Field emission scanning electron microscopy (FE-SEM) image and energy dispersive spectroscopy (EDS) of chromium(III) terephthalate metal-organic frameworks (MIL-101(Cr)). **b** N_2 adsorption curve of MIL-101(Cr). **c** Isothermal water adsorption curve of MIL-101(Cr). **d** Dynamic water sorption cycles of MIL-101(Cr) at 23 °C. **e** Solubility variation with temperature of ammonium nitrate, which presents the energy density of ammonium nitrate at 722 kJ kg^{-1} within the operating temperature range of 5–50 °C. Source data are provided as a Source Data file.

the temperature variation under conditions where a constant heat flux is supplied. When latent cooling or endothermic reaction cooling is considered as a heat sink term in the transient energy balance equation, it leads to a non-linear implicit solution. Therefore, the heat dissipation performance of the WD-ER unit is analyzed by using the simplified term of effective specific heat capacity as in Eq. (11) where m_c represents the mass of the carrier, c_{ep} denotes the effective specific heat capacity, T is the temperature, and Q_{net} represents the net heat transfer to the exterior, respectively. The carrier is defined as a material that absorbs and desorbs the working medium (the charging and discharging of the passive isothermal film are governed by a chain reaction within the WD-ER unit, which requires a temperature change):

$$m_c \cdot c_{ep} \cdot (T_{i+1} - T_i) = Q_{net} \quad (11)$$

The effective specific heat capacity is presented in Fig. S12 and Eqs. (S1)–(S5), which is calculated based on the characteristics of the WD-ER unit. The experimental data in Fig. 5a can be predicted with a maximum error of 8.4% using effective specific heat capacity. Figure 5b displays the cooling energy density of the WD-ER unit in terms of

https://doi.org/10.1038/s41467-024-52328-z

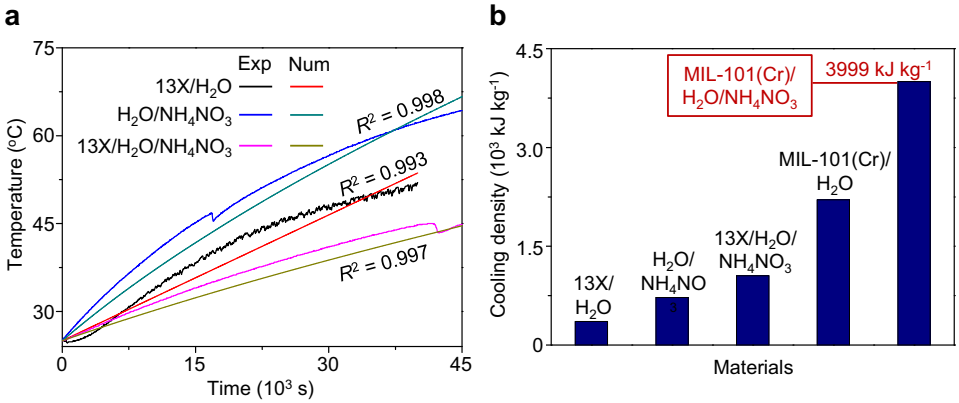

Fig. 5 | Practical performances of the water desorption-driven endothermic reaction (WD-ER) unit. a Verification of numerical analysis during the heat dissipation process. The accuracy of the predicted values with respect to the experimental data is represented as the R^2 value. **b** Cooling energy density. 13X and MIL-101(Cr) represent the zeolite 13X and chromium(III) terephthalate metal-organic frameworks, respectively. Source data are provided as a Source Data file.

materials. The zeolite 13X/H_2O/NH_4NO_3 achieves the cooling energy density of 1052 kJ kg^{-1} within the temperature range of 5–50 °C as proposed in the previous research[12]. However, the latent cooling of MIL-101(Cr) presents the cooling energy density of 2206 kJ kg^{-1}. It is attributed to significantly higher working capacity of 2.06 g g^{-1} compared to that of zeolite 13X (0.24 g g^{-1}). Moreover, the desorption enthalpy of MIL-101(Cr) is higher than that of zeolite 13X (27.4 kJ mol^{-1}). Consequently, the cooling energy density of the WD-ER unit composed of MIL-101(Cr)/H_2O/NH_4NO_3 reaches 3999 kJ kg^{-1}.

Note that the solubility and dissolution enthalpy data for the solute pairs as a function of temperature are presented in Fig. S13. Although potassium bromate ($KBrO_3$) exhibits a high dissolution enthalpy in water at −40.1 kJ mol^{-1}, the cooling energy density is significantly lower in that its solubility is only one-fourth that of ammonium nitrate. Within the operating temperature range of 5–50 °C, ammonium nitrate has the highest energy density at 722 kJ kg^{-1}. Furthermore, MIL-101(Cr) is reported for its exceptional energy density in moisture adsorption-cooling applications[29].

Practical applications

The manufacturing process of the passive isothermal film is summarized in Fig. 6a. Ammonium nitrate crystals were dispersed into a waterproof surface and a moisture environment was formed. A SiO_2/Ti/Ag/PDMS film coated on the back with MIL-101(Cr) was attached to H_2O/NH_4NO_3 layer. The dimensions of the passive isothermal film consist of PDMS (230 µm), SiO_2/Ti/Ag (525 µm) and a WD-ER unit (950 µm). The mass ratios of MIL-101(Cr), water, and ammonium nitrate in the WD-ER unit are 0.4, 1.0, and 0.53, respectively. The temperature variation of the passive isothermal film was tested throughout a full day under various climatic conditions (Table 1 and Fig. S14). As the result of the experiment in Seoul is presented in Fig. 6b, the temperature of white paint increases to 52.5 °C during the daylight hours and drops to 0.8 °C at night. The maximum temperature of the radiative cooling unit is 35.8 °C, which is 16.7 °C lower than the white paint. However, the significant heating load is still required to achieve 25 °C at night. The passive isothermal film demonstrates a reduction of 4.8 °C in the maximum daytime temperature compared to the radiative cooling unit, while presenting a significant increase of the nighttime temperature by 13.6 °C. It allows for a reduction of the cooling load by −4 kJ kg_{air}^{-1} and heating load by 13.7 kJ kg_{air}^{-1}, even without considering humidity. The relatively large temperature difference of 17.5 °C is attributed to the difficulty of preserving equilibrium between the charging and discharging of the WD-ER unit, especially due to the relatively short daytime duration in the test region compared to nighttime. In Fig. 6b, the maximum cooling power during the daylight hours reaches −0.53 kW m^{-2}, while the heating power is 0.31 kW m^{-2} (the cooling and heating power of the passive isothermal film was obtained by calculating the power required to maintain the temperature difference between the indoor air in the system with white paint surface and that with passive isothermal film).

The result from tests conducted at the White Sand Dunes in Vietnam indicates that the temperature of white paint rises to 76.0 °C during the daylight hours and drops to 11.8 °C at night, resulting in a temperature difference of 64.2 °C. Although the radiative cooling unit reduces the maximum temperature to 42.5 °C, the minimum temperature at night is lower than that of white paint due to the thermal emission. The passive isothermal film significantly reduces the maximum temperature difference to 14.1 °C and generates a cooling power of −1.1 kW m^{-2} during the daytime and a heating power of 0.28 kW m^{-2} at nighttime. By integrating the heating and cooling power generated throughout a full day and adding the solar energy absorbed by the white paint, the diurnal energy balance is established with an error margin of 9.7%, demonstrating the reliability of the experimental results (this analysis is valid for results from all regions). The thermal resistances for analyzing heat transfer due to the medium are presented in Fig. S15, and the calculated values are given in Eqs. (S6)–(S25). As presented in Table S1 at the White Sand Dunes, the medium heat transfer of white paint is −4.33 W, in which the temperature is higher than that of the ambient air, resulting from heat loss to the outside. The net radiation power is 4.28 W. This suggests a thermal equilibrium, which is consistent with the stable temperature as in Fig. 6. In contrast, the passive isothermal film presents a net heat transfer of 0.507 W, corresponding to the temperature increase in Fig. 6, which is used for charging of the WD-ER unit.

Note that previous studies on radiative coolers were conducted in test beds with insulating materials and air pockets to minimize the influence of external convection[2,3,6,8,30–33]. However, this study was conducted under extreme conditions with only a passive isothermal film attached to a polyethylene film on the upper surface without an air pocket. Designing the air pocket may not be feasible when applying the passive isothermal film to building envelopes. If the test had included an air pocket, a lower temperature difference of the passive isothermal film would have been obtained, resulting from the improved overall thermal resistance. The performance of the passive isothermal film is independent of installation angles as its optical properties in the UV-Vis-NIR region remain almost constant regardless of the angle of irradiation. In addition, overall thermal resistances increase in proportion to the indoor space volume, which could reduce daily maximum temperature differences. In other words, the effectiveness of the passive isothermal film will be more noticeable when applied to an actual building envelope.

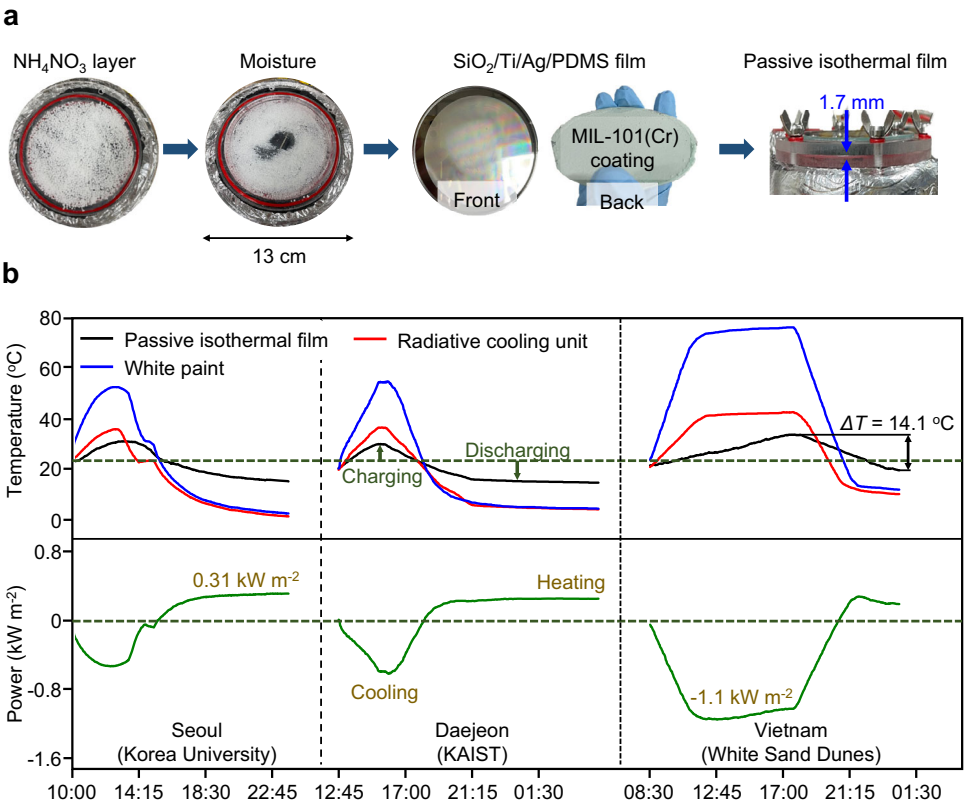

Fig. 6 | Demonstration of the passive isothermal film. a Images of the passive isothermal film composed of the radiative cooling unit and the water-desorption driven endothermic reaction (WD-ER) unit. **b** Temperature variation and cooling/heating power of the passive isothermal film throughout a full day. PDMS and MIL-101(Cr) represent the polydimethylsiloxane and chromium(III) terephthalate metal-organic frameworks, respectively. ΔT represents the difference between the maximum and minimum temperature in a day. Source data are provided as a Source Data file.

Discussion

This study demonstrated a millimeter-scale passive isothermal film capable of maintaining temperatures close to 25 °C in arid climates characterized by significant daily temperature fluctuations, without relying on energy consumption and solely utilizing natural processes. The passive isothermal film consists of a radiative cooling unit, incorporating polydimethylsiloxane (PDMS) with a diffraction grating and fused SiO_2/Ti/Ag sublayers, and a water desorption-driven endothermic reaction (WD-ER) unit. During the daylight hours, thermal emission is induced by constructive interference at wavelengths around 9.2 µm within the PDMS diffraction grating, which corresponds to a peak wavelength of a black body at 40 °C. The diffraction grating features protrusions of 3.25 µm in width and height arranged at 8 µm intervals. The fused SiO_2/Ti/Ag film primarily reflects solar energy in the ultraviolet-visible range. Net thermal energy is consumed in charging the WD-ER unit, involving the desorption of water from chromium(III) terephthalate metal-organic frameworks (latent cooling) and the dissolution of ammonium nitrate in water (endothermic reaction cooling). During the nighttime, the reduced thermal emission from the PDMS diffraction grating minimizes external heat loss, attributed to destructive interference occurring at a wavelength of 10.2 µm, corresponding to peak emission of black body at 10 °C. The reverse thermochemical reaction of the WD-ER unit maintains indoor temperature in response to lower outdoor temperatures. Under the climate conditions where white paint exhibits a temperature difference of 64.2 °C throughout a full day, the passive isothermal film reduces this to 14.1 °C (Note that although radiative coolers previously reported lower daytime temperatures, it leads to a daily temperature difference of 32.4 °C by heat loss at night which requires a substantial heating load in active systems). The passive isothermal film achieves the reductions of approximately −1.1 and 0.3 kW m^{-2} in cooling and heating loads, respectively. These results indicate the potential of designing a passive system suitable for human habitation without the need for an active system.

Methods

Radiative cooling unit

Preparation: a polydimethylsiloxane (PDMS) diffraction grating was designed to generate thermal emission during the daylight hours when temperatures range from 30 to 60 °C, and to suppress thermal emission during the nighttime when temperatures range from −10 to 10 °C. The dimensions of the diffraction grating were set at 3.25 µm, both in width and height, to take advantage of the resonance phenomenon of electromagnetic waves. The thickness of the grating was prepared within the range of 30–100 µm. The design leverages optical diffraction and interference principles to selectively modulate thermal emission in the infrared (IR) region, resulting from the superposition of diffracted waves. To do this, SU-8 was injected into the substrate followed by spin coating and heat curing to obtain a solid SU-8 layer. A designed pattern mask was placed on the cured SU-8 surface and exposed it to ultraviolet (UV) light. After that, SU-8 was dissolved in a solvent, leaving only the patterned structure. The PDMS prepolymer was mixed with a UV curing agent in a 10:1 ratio. It was spin-coated onto the SU-8 mold surface and heat-cured to create the diffraction grating. The fused SiO_2/Ti/Ag film was fabricated using the electron-beam evaporation deposition method. Ti with thickness of 10 nm was coated on a 525 µm fused silica wafer followed by deposition of Ag with 250 nm. The radiative cooling unit was obtained by integrating the fused SiO_2/Ti/Ag film and the PDMS diffraction grating through a plasma deposition process.

Characterization: field emission scanning electron microscopy (FE-SEM) was conducted using a Quanta FEG 240 instrument from FEI.

Table 1 | Data summary for the practical application of the passive isothermal film

Locations	Coordinates	Ambient conditions	White paint	Radiative cooling unit	Passive isothermal film
Korea University, Seoul, South Korea	37.5827, 127.0271	T_{min}: 1.8, T_{max}: 16.1, T_{avg}: 8.4	T_{min}: 0.8, T_{max}: 52.5	T_{min}: −0.1, T_{max}: 35.8	T_{min}: 13.5, T_{max}: 31.0, q_h: 0.31, q_c: −0.53
	37.5827, 127.0275	T_{min}: 5.9, T_{max}: 18.4, T_{avg}: 11.4	T_{min}: 3.1, T_{max}: 51.2	T_{min}: 2.0, T_{max}: 37.4	T_{min}: 14.0, T_{max}: 29.1, q_h: 0.27, q_c: −0.56
KAIST, Daejeon, South Korea	36.375, 127.3567	T_{min}: 6.2, T_{max}: 18.1, T_{avg}: 12.8	T_{min}: 4.3, T_{max}: 54.6	T_{min}: 4.0, T_{max}: 36.5	T_{min}: 14.6, T_{max}: 29.7, q_h: 0.25, q_c: −0.62
Red Sand Dunes, Vietnam	10.9489, 108.296	T_{min}: 15.8, T_{max}: 33.3, T_{avg}: 25.6	T_{min}: 13.0, T_{max}: 72.9	T_{min}: 11.1, T_{max}: 42.0	T_{min}: 19.8, T_{max}: 32.6, q_h: 0.17, q_c: −1.11
White Sand Dunes, Vietnam	11.0749, 108.4293	T_{min}: 14.9, T_{max}: 35.6, T_{avg}: 24.1	T_{min}: 11.8, T_{max}: 76.0	T_{min}: 10.1, T_{max}: 42.5	T_{min}: 19.5, T_{max}: 33.6, q_h: 0.28, q_c: −1.12

T_{min}, T_{max}, and T_{avg} represent the minimum, maximum, and average temperature, respectively, with units in degrees Celsius. q_h and q_c denote the heating and cooling power respectively, with units in kW m^{-2}.

Prior to imaging, the sample underwent pretreatment with a Pt target at 20 mA for 60 s[34,35]. Energy dispersive spectroscopy (EDS) was performed using AZteclive Ultim Max40 equipment from Oxford. Ultraviolet-visible-near infrared (UV-Vis-NIR) transmittance, absorptivity, and transmittance measurements were carried out with JASCO's V-670 instrument. The wavelength range covered 200–2700 nm, with a data interval of 1 nm. The UV-Vis bandwidth was 5.0 nm, and the near infrared bandwidth was 20 nm. The scan speed was set at 200 nm min^{-1}. Fourier transform infrared (FT-IR) analysis was conducted using JASCO's IR4700 instrument. The wavelength range for FT-IR analysis was 2.5–25 µm, with a data interval of 0.964 cm^{-1}. The resolution was 4 cm^{-1}, apodization was set to cosine, and the scanning speed was 2 mm s^{-1}, respectively. X-ray diffraction (XRD) analysis was conducted using a Rigaku MiniFlex 600. The system operated at an X-ray power of 600 W with a copper X-ray tube. Measurements were taken with a step size of 0.02°, covering a range of 5–90°, and the sample holder was 5 mm. For X-ray photoelectron spectroscopy (XPS), a Thermo Fisher Scientific K-ALPHA system was utilized, operating at X-ray irradiation conditions of 12,000 V, 6 mA, and 72 Wd. The analyzer's spatial resolution was set to less than 30 µm (using the knife edge method), and the energy resolution was maintained at less than 0.5 eV.

WD-ER unit

Preparation: chromium(III) nitrate nonahydrate ($Cr(NO_3)_3 \cdot 9H_2O$), terephthalic acid (H_2BDC), N,N-Dimethylformamide (DMF), ethanol, deionized water, 30 wt% sodium silicate solution, 1 mol L^{-1} NaOH solution, and ammonium nitrate (NH_4NO_3) were purchased from Sigma-Aldrich. MIL-101(Cr) was synthesized using the hydrothermal method. A mixture of 4.0 g of chromium(III) nitrate nonahydrate, 1.66 g of terephthalic acid, and 50 g of deionized water was injected into a Teflon-lined stainless steel autoclave. The mixture was heated to 220 °C and maintained for 8 h. Afterward, it was cooled to room temperature through natural air convection and then centrifuged to obtain a highly concentrated mixture. The process of dispersing the mixture in DMF, stirring it for 12 h, and centrifuging was repeated four times to remove the residual substances. The solvent was removed by maintaining the mixture at 50 °C in a convection oven, leaving only the powder, which was then dried in a vacuum at 70 °C to obtain MIL-101(Cr). A mixture of MIL-101(Cr) powder, ethanol, and deionized water was stirred magnetically for 2 h at a mass ratio of 1:6:2. Then, 0.05 wt% of 30 wt% sodium silicate solution was added to the mixture, which was stirred for an additional 24 h. The back of the SiO_2/Ti/Ag film was coated by injecting the coating mixture using a conical funnel to prevent liquid leakage, and it was maintained at 40 °C in a convection oven for 5 h. It was treated in a vacuum at 70 °C for 12 h to remove gas and impurities adsorbed on MIL-101(Cr). NH_4NO_3 crystals were dispersed to the waterproofed surface, and an appropriate amount of water for the operating temperature range of 5–50 °C was injected to create a moisture environment. A passive isothermal film was formed by attaching a SiO_2/Ti/Ag/PDMS unit coated with MIL-101(Cr) on top of the NH_4NO_3 and moisture layers (NH_4NO_3/water/MIL-101(Cr) corresponds to the WD-ER layer, while the fused SiO_2/Ti/Ag/PDMS diffraction grating is the radiative cooling layer).

Characterization: field emission scanning electron microscopy (FE-SEM) was carried out using a Quanta FEG 240 by FEI. The sample was pretreated with a Pt target at 20 mA for 60 s. Energy dispersive spectroscopy (EDS) was performed using AZteclive Ultim Max40 (Oxford). Transmission electron microscopy (TEM) measurements were carried out using the FEI Tecnai F20 G2. The microscope operated with an acceleration voltage range of 50–200 kV, achieving an image resolution of 0.23 nm or better, and magnification capabilities from 25 to 1,030,000. Prior to measurement, the samples underwent a 2-h ultrasonication process. The N_2 adsorption curve was evaluated with Micromeritics' TriStar II 3020 equipment, where the bath temperature was −195.9 °C (nitrogen saturation temperature), and the equilibrium interval was 10 s. The surface area was calculated from the N_2 adsorption curve using Brunauer–Emmett–Teller theory. Dynamic vapor sorption was measured with Measurement Systems' DVS Intrinsic PLUS. Water sorption performance was measured with 3Flex from Micromeritics.

Performance evaluation

A test space with an inner diameter of 90 mm and a height of 50 mm was constructed to evaluate the practical performance of the passive isothermal film. A 20 mm thick extrusion insulation plate with a thermal conductivity of 0.03 W m^{-1} K^{-1} was placed around the sides to minimize heat loss. The average overall heat transfer coefficient was 0.015 W K^{-1} by considering the inner space (natural convection), insulating materials (conduction), and the ambient environment (intermittent forced/natural convection). A passive isothermal film with diameter of 90 mm was installed on the upper surface and fastened with a clamp to ensure the complete sealing. A low-density polyethylene film was applied to the upper surface to minimize heat transfer from the external air and direct contact with contaminants and humidity. Data were collected using Autonics' KRN1000 data logger and type K thermocouples were utilized to measure the temperature of the internal space. The data interval was set to 1 s, and the temperature measurement uncertainty was less than 0.1 °C. During the outdoor testing, 12 V and 100 Ah capacity battery was connected to an inverter to provide a stable power supply for the data logger. Tests were conducted in various regions as summarized in Table 1 to investigate the impact of climate conditions.

Data availability

All data supporting the findings of this study are available within the article and Supplementary Information files. All data are available from the corresponding author upon request. Source data are provided with this paper.

References

1. Kim, S. et al. Indoor CO_2 capture-driven passive cooling for photovoltaics with ventilation energy reduction utilizing amine-functionalized adsorbents. *Energy Convers. Manag.* **307**, 118351 (2024).

2. Raman, A. P., Anoma, M. A., Zhu, L., Rephaeli, E. & Fan, S. Passive radiative cooling below ambient air temperature under direct sunlight. *Nature* **515**, 540–544 (2014).
3. Wang, T. et al. A structural polymer for highly efficient all-day passive radiative cooling. *Nat. Commun.* **12**, 365 (2021).
4. Zhou, L. et al. A polydimethylsiloxane-coated metal structure for all-day radiative cooling. *Nat. Sustain.* **2**, 718–724 (2019).
5. Li, T. et al. A radiative cooling structural material. *Science* **364**, 760–763 (2019).
6. Xiang, B. et al. 3D porous polymer film with designed pore architecture and auto-deposited SiO_2 for highly efficient passive radiative cooling. *Nano Energy* **81**, 105600 (2021).
7. Kim, H. et al. Adsorption-based atmospheric water harvesting device for arid climates. *Nat. Commun.* **9**, 1191 (2018).
8. Wang, Z. et al. Lightweight, passive radiative cooling to enhance concentrating photovoltaics. *Joule* **4**, 2702–2717 (2020).
9. Wang, C. et al. A thermal management strategy for electronic devices based on moisture sorption-desorption processes. *Joule* **4**, 435–447 (2020).
10. Yu, W., Zhang, G., Liu, C. & Fan, S. Hard carbon nanotube sponges for highly efficient cooling via moisture absorption–desorption process. *ACS Nano* **14**, 14091–14099 (2020).
11. Lu, Z., Strobach, E., Chen, N., Ferralis, N. & Grossman, J. C. Passive sub-ambient cooling from a transparent evaporation-insulation bilayer. *Joule* **4**, 2693–2701 (2020).
12. Kim, S., Park, J. H., Lee, J. W., Kim, Y. & Kang, Y. T. Self-recovering passive cooling utilizing endothermic reaction of NH_4NO_3/H_2O driven by water sorption for photovoltaic cell. *Nat. Commun.* **14**, 2374 (2023).
13. Wang, W. W. et al. Thermo-hydrodynamic analytical model, numerical solution and experimental validation of a radial heat pipe with internally finned condenser applied for building heat recovery units. *Energy Convers. Manag.* **219**, 113041 (2020).
14. Tang, H. et al. Review of applications and developments of ultra-thin micro heat pipes for electronic cooling. *Appl. Energy* **223**, 383–400 (2018).
15. Zhou, J. et al. Vacuum insulation arrays as damage-resilient thermal superinsulation materials for energy saving. *Joule* **6**, 2358–2371 (2022).
16. Joshi, B. et al. Electrostatically sprayed nanostructured electrodes for energy conversion and storage devices. *Adv. Funct. Mater.* **31**, 2008181 (2021).
17. An, S., Joshi, B., Yarin, A. L., Swihart, M. T. & Yoon, S. S. Supersonic cold spraying for energy and environmental applications: one-step scalable coating technology for advanced micro-and nanotextured materials. *Adv. Mater.* **32**, 1905028 (2020).
18. Sadhishkumar, S. & Balusamy, T. Performance improvement in solar water heating systems—a review. *Renew. Sustain. Energy Rev.* **37**, 191–198 (2014).
19. Sergei, K., Shen, C. & Jiang, Y. A review of the current work potential of a trombe wall. *Renew. Sustain. Energy Rev.* **130**, 109947 (2020).
20. de Araujo Passos, L. A., van den Engel, P., Baldi, S. & De Schutter, B. Dynamic optimization for minimal HVAC demand with latent heat storage, heat recovery, natural ventilation, and solar shadings. *Energy Convers. Manag.* **276**, 116573 (2023).
21. Faraj, K., Khaled, M., Faraj, J., Hachem, F. & Castelain, C. Phase change material thermal energy storage systems for cooling applications in buildings: a review. *Renew. Sustain. Energy Rev.* **119**, 109579 (2020).
22. Kim, S. et al. CO_2 capture-driven thermal battery using functionalized solvents for plus energy building application. *Energy Convers. Manag.* **260**, 115606 (2022).
23. Fei, J. et al. Switchable surface coating for bifunctional passive radiative cooling and solar heating. *Adv. Funct. Mater.* **32**, 2203582 (2022).
24. Du, L. et al. Highly efficient subambient all-day passive radiative cooling textiles with optically responsive MgO embedded in porous cellulose acetate polymer. *Chem. Eng. J.* **469**, 143765 (2023).
25. Li, D. et al. Scalable and hierarchically designed polymer film as a selective thermal emitter for high-performance all-day radiative cooling. *Nat. Nanotechnol.* **16**, 153–158 (2021).
26. Liu, X. et al. Biomimetic photonic multiform composite for high-performance radiative cooling. *Adv. Opt. Mater.* **9**, 2101151 (2021).
27. Lin, C. et al. A solution-processed inorganic emitter with high spectral selectivity for efficient subambient radiative cooling in hot humid climates. *Adv. Mater.* **34**, 2109350 (2022).
28. Zhu, B. et al. Subambient daytime radiative cooling textile based on nanoprocessed silk. *Nat. Nanotechnol.* **16**, 1342–1348 (2021).
29. Xu, J. et al. Sustainable moisture energy. *Nat. Rev. Mater.* **1**, 1–16 (2024).
30. Zeng, S. et al. Hierarchical-morphology metafabric for scalable passive daytime radiative cooling. *Science* **373**, 692–696 (2021).
31. Leroy, A. et al. High-performance subambient radiative cooling enabled by optically selective and thermally insulating polyethylene aerogel. *Sci. Adv.* **5**, eaat9480 (2019).
32. Zhang, X. et al. A moisture-wicking passive radiative cooling hierarchical metafabric. *ACS Nano* **16**, 2188–2197 (2022).
33. Tian, Y. et al. Superhydrophobic and recyclable cellulose-fiber-based composites for high-efficiency passive radiative cooling. *ACS Appl. Mater. Interfaces* **13**, 22521–22530 (2021).
34. Kim, S., Kim, M., Xu, Z., Wang, R. & Kang, Y. T. Hybrid energy-harvesting device driven by membrane-based CO_2 capture. *Cell Rep. Phys. Sci.* **4**, 12 (2023).
35. Kim, S. et al. Sustainable energy harvesting from post-combustion CO_2 capture using amine-functionalized solvents. *Energy* **267**, 126532 (2023).

Acknowledgements

This study was supported by a National Research Foundation of Korea (NRF) grant funded by the Korean government (MSIT) (No. NRF-2020R1A5A1018153).

Author contributions

S.K. performed data curation, investigation, experimental/theoretical analysis, and writing. S.L. and J.L. conducted data curation and experimental analysis. H.W.C. carried out theoretical analysis and discussion. W.C. conducted investigation and discussion. Y.T.K. supervised conceptualization, methodology, writing review, and editing.

Competing interests

The authors declare no competing interests.

Additional information

Supplementary information The online version contains supplementary material available at https://doi.org/10.1038/s41467-024-52328-z.

Correspondence and requests for materials should be addressed to Yong Tae Kang.

Peer review information *Nature Communications* thanks Hong Ye, Tingxian Li, and the other, anonymous, reviewer(s) for their contribution to the peer review of this work. A peer review file is available.